ESAIM: M2AN 53 (2019) 1695–1713
https://doi.org/10.1051/m2an/2019036

ESAIM: Mathematical Modelling and Numerical Analysis
www.esaim-m2an.org

NEW VOLUME CONSISTENT APPROXIMATION FOR BINARY BREAKAGE POPULATION BALANCE EQUATION AND ITS CONVERGENCE ANALYSIS

Mehakpreet Singh[1,*], Themis Matsoukas[2], Ahmad B. Albadarin[1] and Gavin Walker[1]

Abstract. This work is focused on developing a numerical approximation based on finite volume scheme to solve a binary breakage population balance equation (PBE). The mathematical convergence analysis of the proposed scheme is discussed in detail for different grids. The proposed scheme is mathematical simple and can be implemented easily on general grids. The numerical results and findings are validated against the existing scheme over different benchmark problems. All numerical predictions demonstrate that the proposed scheme is highly accurate and efficient as compared to the existing method. Moreover, the theoretical observations concerning order of convergence are verified with the numerical order of convergence which shows second order convergence irrespective of grid chosen for discretization. The proposed scheme will be the first ever numerical approximation for a binary breakage PBE free from that the particles are concentrated on the representative of the cell.

Mathematics Subject Classification. 35R09, 65R20.

Received November 20, 2018. Accepted May 7, 2019.

1. Introduction

Breakage process is a size reduction mechanism in particle technology which plays very important role in many applications of engineering and sciences [2,4,11,22,28]. The importance of this process lies in those systems where particles continuously change with respect to size (linear dimension, mass or volume). During this process, the total mass remains constant whereas the the total number of the particles in the system gradually increases with time. Breakage is characterized by two functions, the rate of breakage, and the distribution of fragments as shown in Figure 1. Many systems of practical interest are described by a breakage rate that is first order in the concentration of particles. This mechanism represents the disintegration of a cluster or granule during its interaction with its environment, and also serves as a model of polymer degradation (depolymerization) [8, 23, 34].

In this work, we mainly focused on binary breakage process which is mathematically classified as a linear intergo-partial differential equation described by Ziff and McGrady [34] is given as follows:

Keywords and phrases. Particles, binary breakage, population balance equation, finite volume scheme, nonuniform grids.

[1] Bernal Institute, Department of Chemical Science, University of Limerick, V94 T9PX Limerick, Ireland.

[2] 8H Thomas, Department of Chemical Engineering, Pennsylvania State University, State College, PA 16802, USA.

*Corresponding author: Mehakpreet.Singh@ul.ie, singhmehakpreet@gmail.com

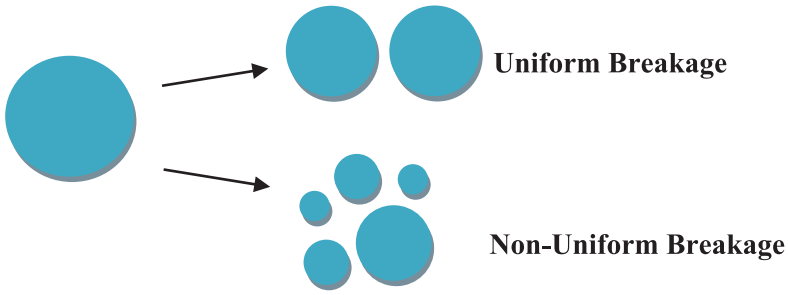

FIGURE 1. Schematic representation of binary and k-nary breakage processes.

$$\frac{\partial G(x,t)}{\partial t} = 2\int_x^\infty F(x, y-x)G(y,t)\mathrm{d}y - G(x,t)\int_0^x F(x-y,y)\mathrm{d}y, \tag{1.1}$$

subject to a initial condition

$$G(x,0) = G_0(t)\ \forall\ x \in (0,\infty). \tag{1.2}$$

In the equation (1.1), $G(x,t)$ expresses the number density function of volume $x > 0$ at a given time $t \geq 0$, that is, the number of particles in the infinitesimal range $[x, x+dx]$ at any time t is given by $G(x,t)\mathrm{d}x$ (we take x to refer to the volume of the particle). The breakage kernel $F(x,y)$ describes the rate of breakage of parent particles of volume $x+y$ into fragments of volume x and y and is symmetric and non-negative function of its arguments. The first integral in equation (1.1) accounts for the birth of particles of volume x in the system due to the fragmentation of bigger particles. The second integral accounts for the disappearance of particles of volume x due to formation of the fragments of volume $x-y$ and y. Due to the symmetric property of F, either of the resulting fragments in first integral can form a particle of volume x which needs the factor 2 to account for those formation of the particles. Without loss of generality, the quantities defined in equation (1.1) are taken in dimensionless form [28].

Various other properties such as total number of particles and total mass in the system also play significant role in determining the average particle size and the width of its distribution as described in Omar and Rohani [27] and Kaur *et al.* [12]. These properties defined by moments can be estimated mathematically using the relation given below:

$$\mu_j(t) = \int_0^\infty x^j G(x,t)\mathrm{d}x, \tag{1.3}$$

where $\mu_j(t)$ signifies zeroth order moment (total number of particles) for $j = 0$ and represents first order moment (total mass) for $j = 1$. The binary breakage equation (1.1) can be translated into moment equation by multiplying it with x^j, taking integral from 0 to ∞ and changing the order of the integration:

$$\frac{\mathrm{d}\mu_j(t)}{\mathrm{d}t} = \int_0^\infty G(x,t)\int_0^x (2y^j - x^j)F(x-y,y)\mathrm{d}y\mathrm{d}x. \tag{1.4}$$

Another form of the equation (1.1), known as *volume conservative formulation*, is [3, 26]

$$x\frac{\partial G(x,t)}{\partial t} = \frac{\partial}{\partial x}\left[\int_0^x \int_0^{x-u} uF(u,v)G(u+v)\mathrm{d}v\mathrm{d}u\right]. \tag{1.5}$$

Using the definition of Leibnitz's rule for differentiation under the integral sign and symmetric property of F, it can be easily shown that both relations (1.1) and (1.5) are equivalent.

Many numerical schemes for approximating the equations (1.1) and (1.5) have been proposed in the literature. They include sectional methods [9, 13, 16], finite element methods [7, 25, 33], finite volume schemes [3, 17, 18, 26, 30, 32] and stochastic schemes [19, 20, 24]. Sectional methods are well known for their accuracy but their formulation is complex. However, a sectional technique developed by Attarakih *et al.* [1] is simpler than the existing sectional fixed pivot technique but based on the assumption that particles are concentrated at the representative of the cell. Stochastic methods are also highly accurate but also computationally very expensive. Finite volume schemes are mathematically straightforward and computationally less expensive. These numerical methods also have the ability to compute the number density function and various order moments accurately. Both sectional and finite volume methods assume particles to be concentrated at the representative of the cell. In general, however, the possibility of formation of new particles of different sizes in a given cell is high. To overcome this issue, sectional methods redistribute the particle properties to the neighboring nodes in order to predict the integral moments accurately, whereas finite volume schemes introduce weights to conserve the required properties.

A recent finite volume method by Forestier-Coste and Mancini [6] was built on the basis of allowing overlapping between cells so that particles are no longer required to be concentrated at the representative of the cell. The overview of the numerical scheme developed by Forestier-Coste and Mancini [6] is given as: Suppose merging of cells j and k is denoted by a new cell $(j+k)$ with the lower and upper boundaries as $x_{j-1/2}+x_{k-1/2}$ and $x_{j+1/2}+x_{k+1/2}$, respectively. In the case of a nonuniform mesh, for given cells j and k, there does not, in general, exist a cell i such that $i=j+k$. This shows that cell i will intersect with more than one cell. Therefore, to introduce the notion of overlapping, Forestier-Coste and Mancini [6] added a proportionality constant into the discrete equation (refer to Eq. (A.5) in Appendix A). Their priority was to conserve only the total mass in the system by modifying the aggregation kernel. However, the major drawback of this numerical method is that they restricted (or stopped) the simulations when 2% of the mass leave the system. The detailed description of the method can be found in Appendix A.

This motivates our development of a new mass conserving numerical tool for approximating a binary breakage PBE using the notion of the overlapping of the cells and overcoming the issues of existing method [6]. For the conservation of mass property, some weights are added to the mathematical formulation and no constraints will be imposed on the simulations. In contrast to the numerical scheme of Forestier-Coste and Mancini [6], no modification in binary breakage kernel will be done, however, the important property such as mass conservation law is accomplished by adding weights to the formulation.

The rest of the article is structured as follows: Section 2 deals with the derivation of the proposed scheme. In Section 3, the complete mathematical analysis of the new proposed scheme is discussed. Section 4 is devoted to testing the accuracy of the new scheme against existing scheme. Finally, Section 5 provides the conclusions of the study.

2. New formulation

The concept of overlapping of the cells was first introduced by Forestier-Coste and Mancini [6] to solve a pure aggregation PBE. In this work, we are adapting this concept to derive the mathematical formulation of the new finite volume scheme for approximating a binary breakage PBE which also overcome some issues related to the aggregation PBE discussed earlier. Before the derivation, it is important to note that the volume range x in equation (1.1) contains ∞ in the upper limit which is not appropriate to derive the formulation. So, we fix the computational domain and replace the upper limit with a big positive, say $x_{\max}$ and hence, the truncated equation takes the following form:

$$\frac{\partial G(x,t)}{\partial t} = 2\int_x^{x_{\max}} F(x,y-x)G(y,t)\mathrm{d}y - G(x,t)\int_0^x F(x-y,y)\mathrm{d}y, \tag{2.1}$$

with changed initial condition

$$G(x,t) = G_0(t)\ \forall\ x \in (0, x_{\max}]. \tag{2.2}$$

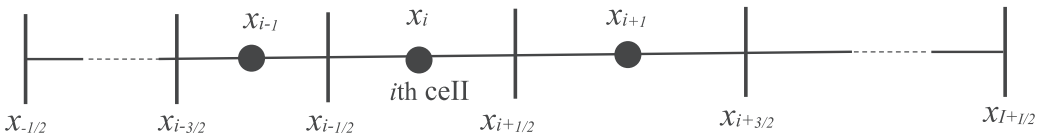

FIGURE 2. One dimensional domain discretization.

We discretize the continuous computational domain $D := (0, x_{\max}]$ into I number of cells as shown in Figure 2. The mean and step size of the ith cell are $x_i = \dfrac{x_{i+1/2} + x_{i-1/2}}{2}$ and $\Delta x_i = x_{i+1/2} - x_{i-1/2}$, respectively.

The number of particles in ith cell is denoted by $N_i(t)$ is

$$N_i(t) = \int_{x_{i-1/2}}^{x_{i+1/2}} G(x,t)\mathrm{d}x. \tag{2.3}$$

By integration of equation (2.1) over the boundaries of the ith cell we obtain the set of ordinary differential equations:

$$\frac{\mathrm{d}N_i}{\mathrm{d}t} = B_i - D_i, \tag{2.4}$$

with initial condition

$$N_i^{in} = N_i(0) = \int_{x_{i-1/2}}^{x_{i+1/2}} G(x,0)\mathrm{d}x.$$

The birth and death terms are defined as

$$B_i = \int_{x_{i-1/2}}^{x_{i+1/2}} \int_{x}^{x_{i+1/2}} F(x, y-x)G(y,t)\mathrm{d}y\mathrm{d}x, \tag{2.5}$$

and

$$D_i = \int_{x_{i-1/2}}^{x_{i+1/2}} G(x,t) \int_{0}^{x} F(x-y, y)\mathrm{d}y\mathrm{d}x. \tag{2.6}$$

First, simplify the birth term (2.5) by changing the order of integration:

$$\begin{aligned} B_i &= 2\int_{x_{i-1/2}}^{x_{i+1/2}} \int_{x_{i-1/2}}^{y} F(x, y-x)G(y,t)\mathrm{d}x\mathrm{d}y + 2\int_{x_{i+1/2}}^{x_{\max}} \int_{x_{i-1/2}}^{x_{\max}} F(x, y-x)G(y,t)\mathrm{d}x\mathrm{d}y, \\ &= 2\int_{x_{i-1/2}}^{x_{i+1/2}} \int_{x_{i-1/2}}^{y} F(x, y-x)G(y,t)\mathrm{d}x\mathrm{d}y + 2\sum_{k=i+1}^{I} \int_{x_{k-1/2}}^{x_{k+1/2}} \int_{x_{i-1/2}}^{x_{\max}} F(x, y-x)G(y,t)\mathrm{d}x\mathrm{d}y, \end{aligned}$$

and apply the quadrature approximation to the outer integrals leads to the following expression:

$$\begin{aligned} B_i &= 2N_i \int_{x_{i-1/2}}^{x_i} F(x_i - x, x)\mathrm{d}x + 2\sum_{k=i+1}^{I} N_k \int_{x_{i-1/2}}^{p_i^k} F(x_k - x, x)\mathrm{d}x + \mathcal{O}(\Delta x^3), \\ &= 2\sum_{k=i}^{I} N_k \int_{x_{i-1/2}}^{p_i^k} F(x_k - x, x)\mathrm{d}x + \mathcal{O}(\Delta x^3). \end{aligned} \tag{2.7}$$

Here

$$p_i^k = \begin{cases} x_i, & \text{when } k = i, \\ x_{i+1/2}, & \text{otherwise.} \end{cases}$$

Similarly, by application of the quadrature approximation to the death term (2.6), we obtain

$$D_i = N_i \int_0^{x_i} F(x_i - y, y)\mathrm{d}y + \mathcal{O}(\Delta x^3). \tag{2.8}$$

The formulation (2.4) as written does not conserve the volume conservative law [29]. This issue is easily resolved by adding two weights to the formulation. Then the equation takes the following form:

$$\frac{\mathrm{d}\hat{N}_i}{\mathrm{d}t} = 2\sum_{k=i}^{I} \hat{N}_k \varphi_k^b \int_{x_{i-1/2}}^{p_i^k} F(x_k - x, x)\mathrm{d}x - \hat{N}_i \varphi_i^d \int_0^{x_i} F(x_i - y, y)\mathrm{d}y, \tag{2.9}$$

where

$$\varphi_k^b = \frac{1}{2\Phi_i^k}, \tag{2.10}$$

and

$$\varphi_i^d = \begin{cases} \dfrac{\sum_{i=1}^{k} x_i \int_{x_{i-1/2}}^{p_i^k} F(x_k - x, x)\mathrm{d}x}{x_i \int_0^{x_i} F(x_i - x, x)\mathrm{d}x}, & \text{if } \int_0^{x_i} F(x_i - x, x)\mathrm{d}x \neq 0, \\ 1, & \text{otherwise.} \end{cases}. \tag{2.11}$$

Here $\hat{N}_i$ denotes the number of particles in ith cell calculated numerically and Φ_i^k depicts the proportionally constant which accounts for the overlapping of the cells after the binary breakage mechanism takes place.

To understand the concept of overlapping of the cells for a binary breakage process, suppose a particle of volume x_k of kth cell is broken in two particles of volumes x_i and x_{k-i}. Then the lower and upper bounds of the newly formed cell becomes $x_{k-1/2} - x_{(k-i)-1/2}$ and $x_{k+1/2} - x_{(k-i)+1/2}$, respectively. In general, it is unlikely that boundaries of a new particle will fall entirely in one cell, as it will partially overlap with more than one cells. Three possibilities of overlapping of the cells arise and are given below:

- The lower boundary of a cell of newly born particle falls inside the ith cell and upper boundary is outside the ith cell. That is, $x_{i-1/2} < x_{k-1/2} - x_{(k-i)-1/2}$ and $x_{k+1/2} - x_{(k-i)+1/2} > x_{i+1/2}$.
- The upper boundary of a cell of newly born particle falls inside the ith cell and lower boundary is outside the ith cell. That is, $x_{i-1/2} > x_{k-1/2} - x_{(k-i)-1/2}$ and $x_{k+1/2} - x_{(k-i)+1/2} < x_{i+1/2}$.
- The domain of newly born particle of size $x_k - x_{k-i}$ completely falls inside the ith cell. That is, $x_{i-1/2} \leq x_{k-1/2} - x_{(k-i)-1/2}$ and $x_{k+1/2} - x_{(k-i)+1/2} \leq x_{i+1/2}$.

The graphical representation of all possible cases of overlapping of the cells is shown in Figure 3. Mathematically, the overlapping factor Φ_i^k can be calculated by defining the following relation:

$$\Phi_i^k = \frac{\overline{\eta_i^k} - \underline{\eta_i^k}}{\Delta x_k - \Delta x_{k-i}}, \tag{2.12}$$

where $\overline{\eta_i^k} = \min(x_{i+1/2}, x_{k+1/2} - x_{(k-i)+1/2})$ and $\underline{\eta_i^k} = \max(x_{i-1/2}, x_{k-1/2} - x_{(k-i)-1/2})$. Here the terms $\overline{\eta_i^k}$ and $\underline{\eta_i^k}$ define the bounds of the intersection of the cells k and $(k-i)$ with cell i. The overlapping constant Φ_i^k describes the extent of overlapping of the newly formed cell with the ith cell and its value lies between 0 and 1, that is, $0 \leq \Phi_i^k \leq 1$. The equality holds when the newly formed cell falls completely outside ($\Phi_i^k = 0$) or inside ($\Phi_i^k = 1$) the ith cell.

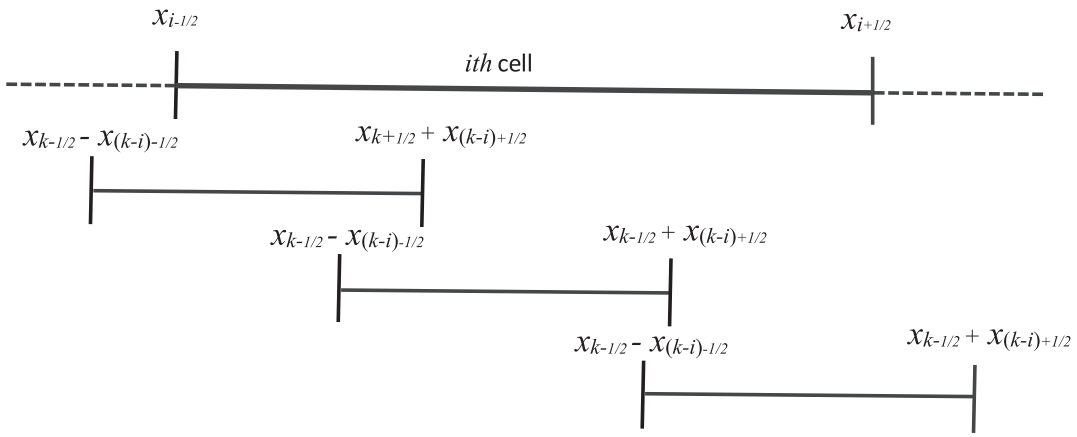

FIGURE 3. Graphical representation of three basic possibilities for overlap.

With the help of aforementioned notations and by adding the proportionality constant corresponding to the overlapping of the cells in equation (2.4), the final expression for a proposed scheme to approximate a binary breakage PBE can be written as

$$\frac{\mathrm{d}\hat{N}_i}{\mathrm{d}t} = 2\sum_{k=i}^{I} \hat{N}_k \Phi_i^k \varphi_k^b \int_{x_{i-1/2}}^{p_i^k} F(x_k - x, x)\mathrm{d}x - \hat{N}_i \varphi_i^d \int_0^{x_i} F(x_i - y, y)\mathrm{d}y. \tag{2.13}$$

Here, the weights φ_k^b and φ_i^d are responsible for volume conservative law and the factor Φ_i^k account for the notion of the overlapping of the cells. It is important to observe that our main aim is to conserve the total volume in the system and no measure has been taken care for the preservation of the zeroth order moment (total number of particles). Therefore, it will be interesting to see to what extent the new scheme predict the zeroth order moment accurately. The theoretical proof the non preservation of the zeroth order moment is provided in Appendix B.

The numerical scheme holds the volume conservative law when it satisfies the following condition:

$$\frac{\mathrm{d}}{\mathrm{d}t}\sum_{i=1}^{I} \hat{N}_i x_i = 0. \tag{2.14}$$

Proposition 2.1. *The proposed numerical scheme* (2.13) *satisfies the volume conservative law.*

Proof. For proving the volume conservation property, multiply the equation (2.13) by x_i which gives

$$\frac{\mathrm{d}}{\mathrm{d}t}\sum_{i=1}^{I} \hat{N}_i x_i = 2\sum_{i=1}^{I} x_i \hat{N}_k \sum_{k=i}^{I} \Phi_i^k \varphi_k^b \int_{x_{i-1/2}}^{p_i^k} F(x_k - x, x)\mathrm{d}x - \sum_{i=1}^{I} x_i \hat{N}_i \varphi_i^d \int_0^{x_i} F(x_i - x, x)\mathrm{d}x. \tag{2.15}$$

Change the order of the summation in the first term and after simplification, we obtain

$$\begin{aligned}\frac{\mathrm{d}}{\mathrm{d}t}\sum_{i=1}^{I} \hat{N}_i x_i &= 2\sum_{k=1}^{I} \hat{N}_k \sum_{i=1}^{k} x_i \Phi_i^k \varphi_k^b \int_{x_{i-1/2}}^{p_i^k} F(x_k - x, x)\mathrm{d}x - \sum_{k=1}^{I} x_k \hat{N}_k \varphi_k^d \int_0^{x_k} F(x_k - x, x)\mathrm{d}x, \\ &= \sum_{k=1}^{I} \hat{N}_k \left[\sum_{i=1}^{k} 2x_i \Phi_i^k \varphi_k^b \int_{x_{i-1/2}}^{p_i^k} F(x_k - x, x)\mathrm{d}x - x_k \varphi_k^d \int_0^{x_k} F(x_k - x, x)\mathrm{d}x \right],\end{aligned}$$

$$= \sum_{k=1}^{I} \hat{N}_k \left[\sum_{i=1}^{k} (2x_i \Phi_i^k \varphi_k^b - x_k \varphi_k^d) \int_{x_{i-1/2}}^{p_i^k} F(x_k - x, x) \mathrm{d}x \right]. \tag{2.16}$$

Using the relation $\sum_{j=1}^{I} \int_{x_{j-1/2}}^{p_j^k} F(x_k - x, x)\mathrm{d}x = \int_0^{x_k} F(x_k - x, x)\mathrm{d}x$ (refer to [31] for detail) and substitute the values of φ_k^b and φ_k^d in equation (2.16), the following can be obtained

$$\frac{\mathrm{d}}{\mathrm{d}t} \sum_{i=1}^{I} \hat{N}_i x_i = \sum_{k=1}^{I} \hat{N}_k \left[\sum_{i=1}^{k} \left(2x_i \Phi_i^k \frac{1}{2\Phi_i^k} - x_k \frac{x_i \int_{x_{i-1/2}}^{p_i^k} F(x_k - x, x)\mathrm{d}x}{x_k \int_0^{x_k} F(x_k - x, x)\mathrm{d}x} \right) \int_{x_{i-1/2}}^{p_i^k} F(x_k - x, x)\mathrm{d}x \right]. \tag{2.17}$$

After cancellation of terms on the right hand side, it can be seen that the coefficient of $\hat{N}_k$ becomes zero, which implies

$$\frac{\mathrm{d}}{\mathrm{d}t} \sum_{i=1}^{I} \hat{N}_i x_i = 0.$$

Hence, the proposed scheme holds the volume conservative law. □

3. Convergence analysis

In this section we use a vector notation to represent the number concentration of particles. Consider the vectors $\mathbf{N} = \{N_1, N_2, \cdots, N_I\}$ and $\hat{\mathbf{N}} = \{\hat{N}_1, \hat{N}_2, \cdots, \hat{N}_I\}$ to represent the exact and numerical values of the number of particles in the system, respectively. The vector form of the discrete equation (2.13) can be written as

$$\frac{\partial \hat{\mathbf{N}}}{\partial t} = \mathbf{J}(\hat{\mathbf{N}}), \quad \hat{\mathbf{N}}(0) = \mathbf{N}(0). \tag{3.1}$$

Here, $\mathbf{J} \in \mathcal{R}^I$ are the functions of $\hat{N}$ with the components

$$\hat{B}_i(\hat{\mathbf{N}}) = 2 \sum_{k=i}^{I} N_k \Phi_i^k \varphi_k^b \int_{x_{i-1/2}}^{p_i^k} F(x_k - x, x)\mathrm{d}x, \tag{3.2}$$

$$\hat{D}_i(\hat{\mathbf{N}}) = N_i \varphi_i^d \int_0^{x_i} F(x_i - y, y)\mathrm{d}y. \tag{3.3}$$

Therefore, the final form of equation is

$$J_i(\hat{\mathbf{N}}) = \hat{B}_i(\hat{\mathbf{N}}) - \hat{D}_i(\hat{\mathbf{N}}). \tag{3.4}$$

The convergence of the discrete system will be shown applying a theorem which will be given further. Firstly, the define the norm L^1 considered for convergence as

$$\|\mathbf{N}(t)\| = \sum_{i=1}^{I} |N_i(t)| \Delta x_i. \tag{3.5}$$

In order to perform the mathematical analysis of the proposed scheme, some definitions and theorems provided by Linz [21], Hundsdorfer and Verwer [10] and Kumar *et al.* [18] will be used.

Definition 3.1. The residual left by substituting the exact solution $\mathbf{N}$ in the discrete system of equations is known as *Spatial Truncation Error*. The mathematical expression for the spatial truncation error is given by

$$\sigma(t) = \frac{\mathrm{d}\mathbf{N}(t)}{\mathrm{d}t} - \mathbf{J}(\mathbf{N}).$$

The numerical scheme is said to be consistent of order p, if $\Delta x \to 0$

$$\|\sigma(t)\| = \mathcal{O}(\Delta x^p), \quad \text{uniformly for all } t,\ 0 \le t \le T.$$

Definition 3.2. The global discretization error for the numerical scheme is the difference between the exact and numerical solution $\epsilon(t) = G(t) - \hat{G}(t)$. The numerical scheme is said to be convergent of order p if, for $\Delta x \to 0$,

$$\|\epsilon(t)\| = \mathcal{O}(\Delta x^p), \quad \text{uniformly for all } t,\ 0 \le t \le T. \tag{3.6}$$

Theorem 3.3. *Let us consider that* $\mathbf{J}$ *is continuous and satisfies the Lipschitz condition*

$$\|\mathbf{J}(\mathbf{f}) - \mathbf{J}(\mathbf{h})\| \le L\|\mathbf{f} - \mathbf{h}\| \text{ for all } \mathbf{f}, \mathbf{h} \in \mathbb{R}^I,\ L < \infty.$$

Then the solution of the semidiscrete system $\mathbf{N}' = \mathbf{J}(\mathbf{N})$ *is nonnegative iff for any vector* $\mathbf{N} \in \mathbb{R}^I$ *and all* $i = 1, 2, \ldots, L$, *and* $t \ge 0$,

$$\mathbf{N} \ge 0, \quad N_i = 0 \Rightarrow J_i(\mathbf{N}) \ge 0.$$

Proof. The generalized proof of the above theorem can be seen in Hundsdorfer and Verwer [10] (Thm 7.1 in Chap. 1). □

Theorem 3.4. *Let us suppose that a Lipschitz condition on* $\mathbf{J}(\mathbf{N})$ *is satisfied for* $0 \le t \le T$ *and for all* $N, \hat{N} \in \mathbb{R}^I$. *That is,* $\boldsymbol{J}$ *satisfies*

$$\|\mathbf{J}(\mathbf{N}) - \mathbf{J}(\hat{\mathbf{N}})\| \le L\|\mathbf{N} - \hat{\mathbf{N}}\|, \quad L < \infty. \tag{3.7}$$

Then a consistent discretization scheme is also convergent and the order of convergence is the same as the order of consistency.

Proof. The detailed proof of this theorem is given in Linz [21]. □

Theorem 3.4 is the main supporting result of this section. Therefore, our aim is to prove that $\hat{\mathbf{J}}(\mathbf{N})$ satisfies the Lipschitz condition (3.7) with respect to the argument $\mathbf{N}$ and that the system given by expression (3.1) is consistent. This result will be followed by the convergence results along with the rate of convergence.

Proposition 3.5. *Let us assume that the* $F(x, y) \in \mathcal{C}^2(]0, x_{\max}]\times]0, x_{\max}]/0$, *respectively. Then for all* $\mathbf{N}$, $\hat{\mathbf{N}}$ $\in \Re^I$, *there exist a constant positive constant* $\beta < \infty$ *such that* $\hat{\boldsymbol{J}}(\mathbf{N})$ *satisfy the Lipschitz condition* (3.7).

Proof. Let us consider

$$\|\mathbf{J}(\mathbf{N}) - \mathbf{J}(\hat{\mathbf{N}})\|_{L^1} = \sum_{i=1}^{I}\sum_{k=i}^{I} |N_k - 2\hat{N}_k\Phi_i^k\varphi_k^b| \int_{x_{i-1/2}}^{p_i^k} F(x_k - x, x)\mathrm{d}x + \sum_{i=1}^{I} |N_k - \hat{N}_k\varphi_i^d| \int_0^{x_i} F(x_i - y, y)\mathrm{d}y.$$

Substitute the values of weights and interchange the sum order, we obtain the following:

$$\begin{aligned}\|\mathbf{J}(\mathbf{N}) - \mathbf{J}(\hat{\mathbf{N}})\|_{L^1} = {} & \sum_{i=1}^{I}\sum_{k=i}^{I} |N_k - \hat{N}_k| \int_{x_{i-1/2}}^{p_i^k} F(x_k - x, x)\mathrm{d}x \\ & + \sum_{i=1}^{I} \left| N_k - \hat{N}_k \frac{\sum_{i=1}^{k} x_i \int_{x_{i-1/2}}^{p_i^k} F(x_k - x, x)\mathrm{d}x}{x_i \int_0^{x_i} F(x_i - x, x)\mathrm{d}x} \right| \int_0^{x_i} F(x_i - y, y)\mathrm{d}y. \end{aligned} \tag{3.8}$$

Further, for all $i \le j$, we have $x_k \le x_i$ and thus the weight φ_i^d

$$\varphi_i^d = \frac{\sum_{i=1}^{k} x_i \int_{x_{i-1/2}}^{p_i^k} F(x_k - x, x)\mathrm{d}x}{x_i \int_0^{x_i} F(x_i - x, x)\mathrm{d}x} \le \frac{x_i \int_0^{x_i} F(x_i - x, x)\mathrm{d}x}{x_i \int_0^{x_i} F(x_i - x, x)\mathrm{d}x} \le 1. \tag{3.9}$$

Now chose a number β in such a way that $\beta = \max_{x\in[0,x_{\max}]} \int_0^x F(x-y, y)\mathrm{d}y$ and rearrange the indices of the second term of equation (3.8) will lead to the following:

$$\|\mathbf{J}(\mathbf{N}) - \mathbf{J}(\hat{\mathbf{N}})\|_{L^1} \le \beta \sum_{k=1}^{I} |N_k - \hat{N}_k| = \beta \|N_k - \hat{N}_k\|_{L^1}.$$

□

Now, our next aim is to prove the main theorem of convergence.

Theorem 3.6. *Suppose that the functions S and b are twice continuously differentiable functions over $(0, x_{\max}]$ and $(0, x_{\max}] \times (0, x_{\max}]$, respectively. Then,*

- *$\hat{\mathbf{N}}$ is non-negative, that is, $\hat{\mathbf{N}} \ge 0$.*
- *the formulation (2.13) is second order consistent, and*
- *the order of convergence of the proposed scheme (2.13) is 2, the independently of the type of grids.*

Proof. For establishing the above theorem, it is necessary to prove the nonnegativity, consistency, and convergence of the solution to the system (2.13). The non-negativity of the numerical scheme is given below:

Non-negativity. For any non-negative number density $\hat{\mathbf{N}} \in \mathbb{R}^I$, (for all $\hat{\mathbf{N}} \ge 0$ whose ith component is zero). So, equations (3.2), and (3.3) give

$$\hat{B}_i(\hat{\mathbf{N}}) \ge 0 \quad \text{and} \quad \hat{D}_i(\hat{\mathbf{N}}) = 0.$$

Equation (3.4) implies $J_i(\hat{\mathbf{N}}) = \hat{B}_i(\hat{\mathbf{N}}) - \hat{D}_i(\hat{\mathbf{N}}) \ge 0$. Moreover, the Theorem 3.3 and Proposition 3.4 imply the non-negativity of the solution for any $i = 1, 2, \ldots, L$.

Consistency. From definition 3.1, the ith component of the spatial truncation error can be written as follows:

$$\sigma_i(t) = \frac{\mathrm{d}N_i(t)}{\mathrm{d}t} - J_i(N_i(t)).$$

Using (2.4) and (3.4), the above equation becomes

$$\sigma_i(t) = \underbrace{B_i - \hat{B}_i}_{T_1} - \underbrace{(D_i - \hat{D}_i)}_{T_2}. \tag{3.10}$$

Now consider the first term T_1 by recalling the relations (3.1) and (3.2) and substituting the value of weight φ_k^b, it is easy to show that

$$B_i - \hat{B}_i = \mathcal{O}(\Delta x^3). \tag{3.11}$$

Now let us discuss the order of consistency of term T_2 similar to the birth term.

$$D_i - \hat{D}_i = N_i(1 - \varphi_i^d) \int_0^{x_i} F(x_i - x, x)\mathrm{d}x + \mathcal{O}(\Delta x^3). \tag{3.12}$$

Now let us simplify the term $1-\varphi_i^d$,

$$1-\varphi_i^d = 1-\frac{\sum_{i=1}^{k} x_i \int_{x_{i-1/2}}^{p_i^k} F(x_k-x,x)\mathrm{d}x}{x_i \int_0^{x_i} F(x_i-x,x)\mathrm{d}x} = \frac{x_i \int_0^{x_i} F(x_i-x,x)\mathrm{d}x - \sum_{i=1}^{k} x_i \int_{x_{i-1/2}}^{p_i^k} F(x_k-x,x)\mathrm{d}x}{x_i \int_0^{x_i} F(x_i-x,x)\mathrm{d}x}. \tag{3.13}$$

Further suppose,

$$I_1 = \int_0^{x_i} xF(x_i-x,x)\mathrm{d}x. \tag{3.14}$$

Replace $x_i - x = v$ and using the definition of symmetry of F, we have

$$I_1 = \int_0^{x_i} (x_i-v)F(v,x_i-v)(-dv) = x_i \int_0^{x_i} F(x_i-x,x) - I_1 \tag{3.15}$$

which further simplifies to

$$x_i \int_0^{x_i} F(x_i-x,x) = 2\int_0^{x_i} xF(x_i-x,x)\mathrm{d}x. \tag{3.16}$$

Using the above relations in equation (3.12) and the rearrangement of terms lead us to the following expression:

$$D_i - \hat{D}_i = \frac{1}{x_i}\left[\int_0^{x_i} xF(x_i-x,x)\mathrm{d}x - \sum_{i=1}^{k} x_i \int_{x_{i-1/2}}^{p_k^i} F(x_i-x,x)\mathrm{d}x\right] = \frac{1}{x_i}\sum_{i=1}^{k}\int_{x_{i-1/2}}^{p_k^i} (x-x_i)F(x_i-x,x)\mathrm{d}x.$$

Now apply the mid-point rule for $i<k$, right-end quadrature for $i=k$ and use the fact that $F(0,.)=0$, we have

$$D_i - \hat{D}_i = \frac{\Theta}{x_i}\sum_{i=1}^{k}\Delta x_j^3,$$

where $\Theta < \infty$ is a finite number. This implies

$$\begin{aligned} D_i - \hat{D}_i &\le \frac{\Theta}{x_i}\Delta x^2 \sum_{i=1}^{k}\Delta x_i = \frac{\Theta}{x_i}\Delta x^2 \frac{x_{i+1/2}}{x_i}, \\ &= \Theta\Delta x^2\Big[\frac{x_i + x_{i+1/2}}{x_i}\Big] = \Theta\Delta x^2\Big[\frac{x_{i-1/2}+x_{i+1/2}}{x_{i-1/2}+x_{i+1/2}}\Big] \le 2\Theta\Delta x^2 = \mathcal{O}(\Delta x^3). \end{aligned} \tag{3.17}$$

Hence,

$$D_i - \hat{D}_i = \mathcal{O}(\Delta x^3). \tag{3.18}$$

Finally, combining the equations (3.11) and (3.18), we get

$$\sigma_i(t) = \mathcal{O}(\Delta x^3),$$

that is,

$$\|\sigma(t)\|_{L^1} = \mathcal{O}(\Delta x^2).$$

Convergence. The consistency result and Proposition 3.5 together provide all the necessary conditions of Theorem 3.4. Therefore, as a result of Theorem 3.4, the formulation (2.13) is second order convergent independently of the type of grid chosen for the discretization. □

4. Numerical comparisons

In this section we verify the accuracy and efficiency of the proposed scheme by comaring with the recently developed finite volume scheme [29] against three different benchmark problems. The comparison is conducted in terms of number density function and integral properties such as zeroth and first order moments. The importance of choosing this particular existing scheme is due to fact that the numerical scheme proposed by Saha *et al.* [29] shows higher accuracy in terms of moments and number density function than the finite volume scheme developed by Bourgade and Filbet [3]. The thorough comparison of the numerical results can be found in Saha *et al.* [29]. It is also important to observe that the numerical results in terms of moments and number density functions were compared only for the exponential initial condition [29]. However, the comparison for our study is demonstrated corresponding to exponential $G(x,0) = e^{-x}$ as well as monodisperse $G(x,0) = \delta(x-1)$ initial conditions. The exact solutions for these conditions are available in Dubovskii *et al.* [5] and Ziff and McGrady [34].

The errors in the number density function is quantified by estimating the weighted sectional error using the following expression:

$$\sigma_i(t) = \frac{\sum_{j=1}^{I} |G_j^{\text{exc}} - G_j^{\text{num}}| x_j^i \Delta x_j^i}{\sum_{j=1}^{I} G_j^{\text{exc}} x_j^i \Delta x_j^i}, \tag{4.1}$$

where $\sigma_i(t)$ for $i = 0$ computes the relative error in the number density function over the given computational domain. Similarly, other order relative sectional errors for the number density function can be calculated. These errors are evaluated for those problems whose exact solutions are available in literature. These errors are calculated at the end of the simulation. The system of discrete set of ODE's are solved using inbuilt `MATLAB` function `ode15s` solver. The numerical simulations are run on machine with specifications *i5 CPU* with *2.40 GHz* and *8 GB RAM*.

The comparison between the numerical and exact results is enhanced by calculating the convergence of the numerical scheme known as *Experimental Order of Convergence* (EOC) for analytically tractable kernels using the following expression [14, 15]:

$$\text{EOC} = \ln\Big(\frac{E_I}{E_{2I}}\Big)/\ln(2), \tag{4.2}$$

where E_I and E_{2I} describes the L^1 error norm calculated by

$$\sum_{j=1}^{I} |G_j^{\text{exc}} - G_j^{\text{num}}| \Delta x_j^i.$$

Here, G_j^{exc} and G_j^{num} describe the number density obtained exactly and numerically, respectively and the symbols I and $2I$ correspond to the number of degrees of freedom.

4.1. Test case I

We begin the comparison of the new and existing numerical schemes with the exact results by considering size independent fragmentation kernel, that is, $F(x,y) = 1$, with initial condition $G(x,0) = \delta(x-1)$. The numerical simulation are run on computational volume domain with $x_{\min} = 10^{-9}$ and $x_{\max} = 1.5$. The given domain is divided into 35 nonuniform grids. The simulations are run till time $t = 1000$ at which the extent of fragmentation is $\dfrac{\mu(t)}{\mu(0)} \approx 52.61$, where $\mu(t)$ is the zeroth moment at time t.

Figure 4 demonstrates the comparison of the numerical results predicted by the proposed (NFVS) and existing (EFVS) schemes against the exact results. It can be observed that the zeroth order moment is in very good agreement with the exact result when computed using the NFVS, whereas, the EFVS shows underprediction

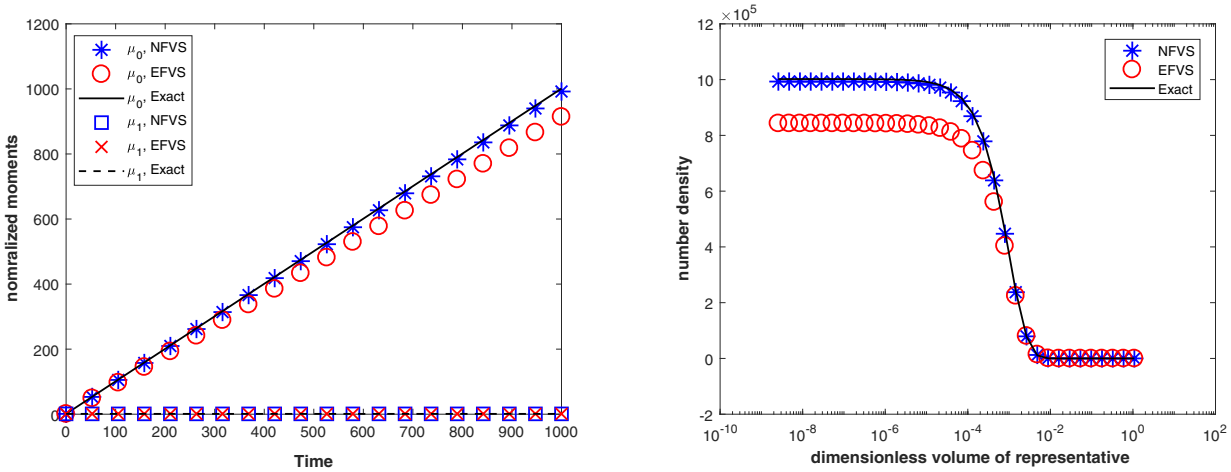

(a) Zeroth and first order moments

(b) Number density function

FIGURE 4. Comparison of normalized moments and number density function corresponding $F(x, y) = 1$ for monodisperse initial condition.

TABLE 1. Weighted error of number distribution for $F(x, y) = 1$ corresponding to monodisperse initial condition.

σ	EFVS 35 cells	NFVS 35 cells	EFVS 70 cells	NFVS 70 cells
σ_0	0.16484	0.11079	0.11849	0.02159
σ_1	0.19995	0.19995	0.12827	0.04275

from the exact results (see Fig. 4a). It is important to note that no measure has been taken for the accurate prediction of zeroth order moment. However, still the proposed scheme has the tendency to track the zeroth order moment with higher precision on a coarse grid of 35 nonuniform cells. As expected, the first order moments approximated by both schemes show excellent agreement with the exact result as shown in Figure 4a, that is, the volume conservative law holds for both schemes. In addition, the qualitative behavior of number density function (in *semilog* scale) is analyzed by plotting it against the volume of the representative (in *logarithmic* scale) in Figure 4b. It reveals that the number density function calculated by the new proposed matches well with the exact results and in contrast to the new scheme, the existing scheme shows under prediction for the number density function.

In order to quantify the errors in the number density function, the weighted sectional errors (4.1) are calculated for a computational domain having 35 as well as 70 nonuniform cells and listed in Table 1. It can be seen from Table that the proposed scheme is highly accurate as it shows approximately 50% less error as compared to the existing scheme. Moreover, these errors are further reduced when both numerical schemes are treated with a refine grid of 70 nonuniform cells, however, still the proposed scheme performs better than the existing scheme. Additionally, Table 2 shows the experimental order of convergence calculated numerically for both uniform and nonuniform grids. It reveals that the proposed scheme shows second order convergence rate similar to the existing scheme irrespective of the type of grid chosen for partitioning the given computational domain. In terms of computational efficiency, the proposed scheme computed all numerical results by consuming lesser CPU time than the existing scheme as shown in Table 3.

TABLE 2. EOC for Test Case I for $F(x, y) = 1$ corresponding to monodisperse initial condition.

Grid points	Uniform grid	Nonuniform grid
30	–	–
60	1.8905	1.9057
120	1.8891	1.9726
240	1.9135	1.9929

TABLE 3. Computational time taken by numerical schemes for $F(x, y) = 1$ corresponding to monodisperse initial condition.

Scheme	Number of cells	Time taken (in s)	Number of cells	Time taken (in s)
EFVS	35	1.2827	70	4.7762
NFVS	35	0.7760	70	1.9669

4.2. Test case II

Similar to the previous test case, the comparison is conducted for size dependent fragmentation kernel, that is, $F(x, y) = x + y$ using monodisperse initial condition. For running the simulations, the same computational and time domain as in the previous case are considered. However, in this case, the extent of fragmentation attained is $\frac{\mu(t)}{\mu(0)} \approx 62.271$.

Figure 5a shows that the zeroth order moment is computed with higher precision by the proposed scheme, however, the same moment is deviating far from the exact result than the one approximated by the existing scheme. Moreover, the first order moment computed by both numerical scheme show equal accuracy, that is, the total volume in the system is conserved in time. Additionally, the qualitative comparison of number density function vs. volume of the representative obtained by both numerical method is illustrated in Figure 5b. It shows that the number density function is more accurately approximated by the proposed scheme than the existing scheme which similar to the previous case shows underpredcition from the exact result . The deviation in the number density function is estimated by quantifying the weighted sectional errors in the number density function for different size grids (see Tab. 4). Again, the proposed scheme shows approximately 50% better accuracy than the existing scheme for both coarse (35 cells) and refined grids (70 cells). The efficiency of the proposed method is also tested in terms of CPU time taken by the numerical methods to obtained all numerical results. Table 5 reveals that the proposed scheme is highly efficient than the existing method as it took lesser time compute the results.

Furthermore, the numerically calculated experimental order of convergence using both uniform and nonuniform grids are listed in Table 6. Similar to the previous case, the proposed scheme shows the convergence rate to be approximately 2 independent of the grids.

4.3. Test case III

In this test problem, the comparison of numerical and exact result is illustrated for the exponential initial condition corresponding to the size dependent fragmentation kernel, that is, $F(x, y) = x+y$. The computational domain begins with $x_{\min} = 10^{-9}$ and $x_{\max} = 1.5$ is divided into 35 nonuniform grids. The time domain is

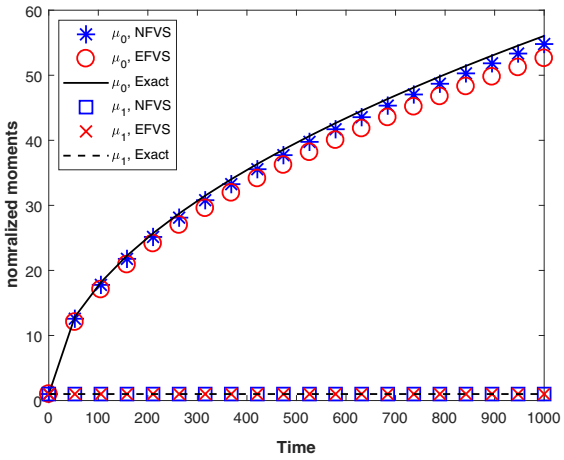

(a) Zeroth and first order moments

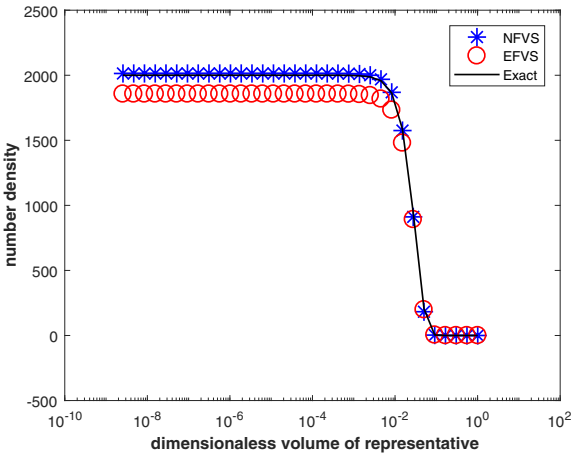

(b) Number Density

FIGURE 5. Comparison of normalized moments and number density for $F(x, y) = x + y$ corresponding to monodisperse initial condition.

TABLE 4. Weighted sectional errors for $F(x, y) = x + y$ corresponding to monodisperse initial condition.

σ	EFVS 35 cells	NFVS 35 cells	EFVS 70 cells	NFVS 70 cells
σ_0	0.11100	0.08323	0.06193	0.02585
σ_1	0.11486	0.11485	0.05430	0.05185

TABLE 5. Computational time taken by numerical schemes for $F(x, y) = x + y$ corresponding to monodisperse initial condition.

Scheme	Number of cells	Time taken (in s)	Number of cells	Time taken (in s)
EFVS	35	1.1240	70	4.5123
NFVS	35	0.7689	70	2.0618

TABLE 6. EOC for Test Case II using $F(x, y) = x + y$ corresponding to monodisperse initial condition.

Grid points	Uniform grid	Nonuniform grid
30	–	–
60	1.8910	1.8163
120	1.9361	1.9437
240	1.9501	1.9853

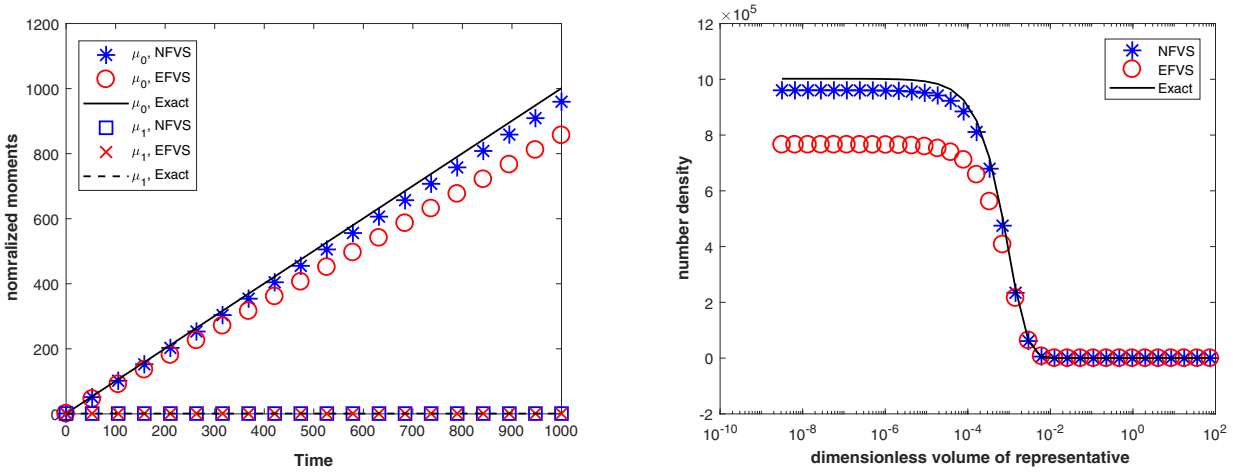

(a) Zeroth and first order moments

(b) Number Density

FIGURE 6. Comparison of normalized moments and number density for $F(x, y) = x + y$ corresponding to exponential initial condition.

TABLE 7. Weighted sectional errors for $F(x, y) = x + y$ corresponding to exponential initial condition.

σ	EFVS 35 cells	NFVS 35 cells	EFVS 70 cells	NFVS 70 cells
σ_0	0.17806	0.05237	0.05211	0.01455
σ_1	0.17717	0.06736	0.05045	0.01957

considered to be the same as in earlier cases, however, the extent of fragmentation attained in this case is $\frac{\mu(t)}{\mu(0)} \approx 20.665$.

The comparison of the number density function and various order moments obtained numerically and exactly are plotted in Figure 6. Once again it can be seen that the time evolution of the zeroth order moment is more accurately captured by the proposed scheme than the existing scheme which shows large deviation from the exact results (see Fig. 6a). However, the prediction of first order moments by both numerical schemes exhibits equal accuracy, that is, the total volume is well captured by both schemes. Moreover, Figure 6b reveals that the number density function plotted against its volume of the representative is estimated with more precision by the proposed scheme than the existing scheme which shows a large deviation from the exact result. Additionally, the quantification of the deviations in the number density functions is captured by calculating the weights sectional errors (4.1) in Table 7. The observations in this case are quite similar to the previous cases as the proposed scheme estimated these errors with higher accuracy than the existing scheme. Moreover, the errors also decrease as the numerical schemes are implemented on a refined grid of 70 nonuniform cells.

In order to check the computational performance of the numerical schemes, the CPU time taken by both schemes to approximate this problem is compared in Table 8. It can be observed that the proposed scheme took less computational time to calculate all numerical results whereas, the existing scheme is consuming more time. Furthermore, the EOC calculated using the proposed scheme is listed in Table 9 corresponding to the both uniform and nonuniform grids. The results reveal that the proposed scheme is second order convergent similar to the cases discussed earlier for monodisperse initial condition.

TABLE 8. Computational time taken by numerical schemes for $F(x, y) = x + y$ corresponding to exponential initial condition.

Scheme	Number of cells	Time taken (in s)	Number of cells	Time taken (in s)
EFVS	35	1.2273	70	2.9669
NFVS	35	0.8035	70	1.5305

TABLE 9. EOC for Test Case III using $F(x, y) = x + y$ corresponding to exponential initial condition

Grid points	Uniform grid	Nonuniform grid
30	–	–
60	1.9057	1.9130
120	1.9726	1.9559
240	1.9929	1.9768

5. Conclusions

In this article, a new approach based on the finite volume scheme is developed for approximating a binary breakage PBE on nonuniform grids. The formulation of the proposed scheme is easy to code, faster to run, and more accurate than the existing scheme. A thorough mathematical analysis is discussed to prove that the proposed scheme is second order convergent. It has been also shown that the proposed scheme is highly accurate in computing the first order moment and the evolution of zeroth order moment with time is captured very well by the proposed scheme. The proposed scheme also presented an improvement with respect to the existing scheme in approximating the number density function. Moreover, the weighted sectional errors estimated by the proposed scheme show approximately 50% more accuracy than the existing scheme. Furthermore, the theoretical observations have been confirmed with the numerical order of convergence to prove that the proposed scheme is second order convergent independently of the type of grid used.

Appendix A. Finite volume scheme for aggregation PBE

This section outlines the mathematical formulation of the existing finite volume scheme [6] for aggregation PBE on non-uniform meshes. The merging of cells i and k is denoted by a new cell $(i + k)$ having lower and upper boundaries as $x_{i-1/2} + x_{k-1/2}$ and $x_{i+1/2} + x_{k+1/2}$, respectively. In the case of a non-uniform mesh, the probability that the merged cells $(i + k)$ exactly falls inside any cell j is very low. This implies that the new cell that is formed after merging can intersect with more than one cell.

We define the following set of indices:

$$S^j = \{(i, k) \in \mathbb{N} \times \mathbb{N} : \ (i + k) \cap j \neq \emptyset\}, \tag{A.1}$$

and

$$R_{i,k} = \{j \in \mathbb{N} : \ j \cap (i + k) \neq \emptyset\}. \tag{A.2}$$

Set S^i expresses mesh couples (i, k) such that their sum intersects the mesh j, whereas set $R_{i,k}$ represents the intersection of the set of meshes j and the sum of the meshes i and k are non-empty.

Further, the time domain is discretized into $t^{p+1} = t^p + \Delta t$ for $p \in \{0, \ldots, N-1\}$. Now let us consider n_j^p is average value of n at time t^p in the cell j, which is an approximation of the number density function $n(x, t^p)$ given by

$$n_j{}^p = \frac{1}{\Delta x_j} \int_{x_{j-1/2}}^{x_{j+1/2}} n(x, t^p)\, \mathrm{d}x, \quad j \in \{1, \ldots, I\}. \tag{A.3}$$

Using the above notations, the finite volume approximation provided by Forestier-Coste and Mancini [6] can be written as

$$n_j^{p+1} = n_j^p + \Delta t \left(\frac{1}{2} \sum_{(i,k)\in S^j} \widehat{K}_{i,k}\; n_i^p\; n_k^p\; \lambda_{i,k}^j \frac{\Delta x_i \Delta x_k}{\Delta x_j} - \sum_{j=0}^{I} K_{j,i}\; n_j^p\; n_i^p \Delta x_i \right), \tag{A.4}$$

where the aggregation kernel $K_{i,k}$ denotes $K_{i,k}= K(x_i, x_k)$ and $\lambda_{i,k}^j$ is a correction factor considered in such a way that it takes the overlapping into account, defined by:

$$\lambda_{i,k}^j = \Big(\frac{\overline{m_{i,k}^j} - \underline{m_{i,k}^j}}{\Delta x_i + \Delta x_k} \Big). \tag{A.5}$$

Here $\overline{m_{i,k}^j}$ and $\underline{m_{i,k}^j}$ indicates the maximum and minimum bounds of the intersection of the cell $i+k$ with a given cell j:

$$\overline{m_{i,k}^j} = \min(x_{j+1/2}, x_{i+1/2} + x_{k+1/2}),$$
$$\underline{m_{i,k}^j} = \max(x_{j-1/2}, x_{i-1/2} + x_{k-1/2}).$$

The formulation derived in equation (A.4) is not volume conserving. In order to achieve the mass conservation property, Forestier-Coste and Mancini [6] have modified the aggregation kernel defined in the first term of the right hand side of equation (A.4) which is given as follows:

$$\widehat{K}_{i,k} = K_{i,k} \frac{2(x_i + x_k)}{\sum_{j\in R_{i,k}} x_j (\lambda_{i,k}^j + \lambda_{k,i}^j)}. \tag{A.6}$$

The modified aggregation kernel ensures that mass conservation law is satisfied. The detailed proof of the mass conservation property and its complete formulation can be found in Forestier-Coste and Mancini [6].

Appendix B. Theoretical proof of non preservation of Zeorth moment

The zeroth order moment is preserved if the following condition is satisfied:

$$\frac{\mathrm{d}}{\mathrm{d}t} \sum_{k=1}^{I} \hat{N}_k = \sum_{k=1}^{I} \hat{N}_k \int_0^{x_k} F(x_k - x, x) \mathrm{d}x. \tag{B.1}$$

Take summation on both side of equation (2.13):

$$\frac{\mathrm{d}}{\mathrm{d}t} \sum_{i=1}^{I} \hat{N}_i = 2 \sum_{i=1}^{I} \hat{N}_k \sum_{k=i}^{I} \Phi_i^k \varphi_k^b \int_{x_{i-1/2}}^{p_i^k} F(x_k - x, x) \mathrm{d}x - \sum_{i=1}^{I} \hat{N}_i \varphi_i^d \int_0^{x_i} F(x_i - x, x) \mathrm{d}x. \tag{B.2}$$

Change the order of the integration in the first term and after simplification to obtain

$$\frac{\mathrm{d}}{\mathrm{d}t}\sum_{i=1}^{I}\hat{N}_i = 2\sum_{k=1}^{I}\hat{N}_k\sum_{i=1}^{k}\Phi_i^k\varphi_k^b\int_{x_{i-1/2}}^{p_i^k}F(x_k-x,x)\mathrm{d}x - \sum_{k=1}^{I}\hat{N}_k\varphi_i^d\int_0^{x_k}F(x_k-x,x)\mathrm{d}x,$$
$$= \sum_{k=1}^{I}\hat{N}_k\left[\sum_{i=1}^{k}2\Phi_i^k\varphi_k^b\int_{x_{i-1/2}}^{p_i^k}F(x_k-x,x)\mathrm{d}x - \varphi_i^d\int_0^{u_k}F(x_k-x,x)\mathrm{d}x\right]. \tag{B.3}$$

Using the relation $\sum_{i=1}^{I}\int_{x_{i-1/2}}^{p_i^k}F(x_k-x,x)\mathrm{d}x = \int_0^{x_k}F(x_k-x,x)\mathrm{d}x$, we get

$$\frac{\mathrm{d}}{\mathrm{d}t}\sum_{i=1}^{I}\hat{N}_i = \sum_{k=1}^{I}\hat{N}_k\sum_{i=1}^{k}(2\Phi_i^k\varphi_k^b-\varphi_k^d)\int_0^{x_k}F(x_k-x,x). \tag{B.4}$$

In order to show the preservation of the zeroth order moment, it is necessary to show that $2\Phi_i^k\varphi_k^b-\varphi_k^d=1$, which is not possible. Hence, this proposed scheme does not preserve the zeroth order moment.

Acknowledgements. The authors gratefully acknowledge the financial support provided by Marie Skłodowska-Curie Individual Fellowship no. 841906 to Dr. Mehakpreet Singh.

References

[1] M.M. Attarakih, H.-J. Bart and N.M. Faqir, Solution of the droplet breakage equation for interacting liquid–liquid dispersions: a conservative discretization approach. *Chem. Eng. Sci.* **59** (2004) 2547–2565.

[2] H. Berthiaux and J. Dodds, A new estimation technique for the determination of breakage and selection parameters in batch grinding. *Powder Technol.* **94** (1997) 173–179.

[3] J.-P. Bourgade and F. Filbet, Convergence of a finite volume scheme for coagulation-fragmentation equations. *Math. Comput.* **77** (2008) 851–882.

[4] A. Braumann, M. Kraft and W. Wagner, Numerical study of a stochastic particle algorithm solving a multidimensional population balance model for high shear granulation. *J. Comput. Phys.* **229** (2010) 7672–7691.

[5] P. Dubovskii, V. Galkin and I. Stewart, Exact solutions for the coagulation-fragmentation equation. *J. Phys. A: Math. General* **25** (1992) 4737.

[6] L. Forestier-Coste and S. Mancini, A finite volume preserving scheme on nonuniform meshes and for multidimensional coalescence. *SIAM J. Sci. Comput.* **34** (2012) B840–B860.

[7] S. Ganesan, An operator-splitting galerkin/supg finite element method for population balance equations: stability and convergence. *ESAIM: M2AN* **46** (2012) 1447–1465.

[8] Y.K. Ho, C. Kirse, H. Briesen, M. Singh, C.-H. Chan and K.-W. Kow, Towards improved predictions for the enzymatic chain-end scission of natural polymers by population balances: the need for a non-classical rate kernel. *Chem. Eng. Sci.* **176** (2018) 329–342.

[9] M. Hounslow, R. Ryall and V. Marshall, A discretized population balance for nucleation, growth, and aggregation. *AIChE J.* **34** (1988) 1821–1832.

[10] W. Hundsdorfer and J.G. Verwer, Numerical solution of time-dependent advection-diffusion-reaction equations. In Vol. 33. Springer Science & Business Media, Berlin (2013).

[11] H.Y. Ismail, M. Singh, S. Darwish, M. Kuhs, S. Shirazian, D.M. Croker, M. Khraisheh, A.B. Albadarin, G.M. Walker, Developing ann-kriging hybrid model based on process parameters for prediction of mean residence time distribution in twin-screw wet granulation. *Powder Technol.* **343** (2019) 568–577.

[12] G. Kaur, M. Singh, T. Matsoukas, J. Kumar, T. De Beer and I. Nopens, Two-compartment modeling and dynamics of top-sprayed fluidized bed granulator. *Appl. Math. Modell.* **68** (2019) 267–280.

[13] S. Kumar and D. Ramkrishna, On the solution of population balance equations by discretization – i. A fixed pivot technique. *Chem. Eng. Sci.* **51** (1996) 1311–1332.

[14] J. Kumar and G. Warnecke, Convergence analysis of sectional methods for solving breakage population balance equations-I: the fixed pivot technique. *Numer. Math.* **111** (2008) 81–108.

[15] J. Kumar and G. Warnecke, Convergence analysis of sectional methods for solving breakage population balance equations-II: the cell average technique. *Numer. Math.* **110** (2008) 539–559.

[16] J. Kumar, M. Peglow, G. Warnecke, S. Heinrich and L. Mörl, Improved accuracy and convergence of discretized population balance for aggregation: the Cell Average Technique. *Chem. Eng. Sci.* **61** (2006) 3327–3342.

[17] R. Kumar, J. Kumar and G. Warnecke, Moment preserving finite volume schemes for solving population balance equations incorporating aggregation, breakage, growth and source terms. *Math. Models Methods Appl. Sci.* **23** (2013) 1235–1273.

[18] J. Kumar, J. Saha and E. Tsotsas, Development and convergence analysis of a finite volume scheme for solving breakage equation. *SIAM J. Numer. Anal.* **53** (2015) 1672–1689.

[19] K. Lee and T. Matsoukas, Simultaneous coagulation and break-up using constant-N monte carlo. *Powder Technol.* **110** (2000) 82–89.

[20] K.F. Lee, R.I. Patterson, W. Wagner and M. Kraft, Stochastic weighted particle methods for population balance equations with coagulation, fragmentation and spatial inhomogeneity. *J. Comput. Phys.* **303** (2015) 1–18.

[21] P. Linz, Convergence of a discretization method for integro-differential equations. *Numer. Math.* **25** (1975) 103–107.

[22] J. Litster and B. Ennis, The Science and Engineering of Granulation Processes. In Vol. 15. Springer Science & Business Media, Berlin (2013).

[23] B.J. McCoy and G. Madras, Discrete and continuous models for polymerization and depolymerization. *Chem. Eng. Sci.* **56** (2001) 2831–2836.

[24] W.J. Menz, J. Akroyd and M. Kraft, Stochastic solution of population balance equations for reactor networks. *J. Comput. Phys.* **256** (2014) 615–629.

[25] M. Nicmanis and M. Hounslow, Finite-element methods for steady-state population balance equations. *AIChE J.* **44** (1998) 2258–2272.

[26] L. Oddershede, P. Dimon and J. Bohr, Self-organized criticality in fragmenting. *Phys. Rev. Lett.* **71** (1993) 3107.

[27] H.M. Omar and S. Rohani, Crystal population balance formulation and solution methods: a review. *Crystal Growth Des.* **17** (2017) 4028–4041.

[28] D. Ramkrishna, Population Balances: Theory and Applications to Particulate Systems in Engineering. Elsevier, Amsterdam (2000).

[29] J. Saha, J. Kumar and S. Heinrich, A volume-consistent discrete formulation of particle breakage equation. *Comput. Chem. Eng.* **97** (2017) 147–160.

[30] J. Saha, J. Kumar and S. Heinrich, On the approximate solutions of fragmentation equations. *Proc. R. Soc. A* **474** (2018) 20170541.

[31] P. Singh and M. Hassan, Kinetics of multidimensional fragmentation. *Phys. Rev. E* **53** (1996) 3134.

[32] M. Singh, J. Kumar, A. Bück and E. Tsotsas, A volume-consistent discrete formulation of aggregation population balance equations. *Math. Methods Appl. Sci.* **39** (2015) 2275–2286.

[33] S. Wu, E.K. Yapp, J. Akroyd, S. Mosbach, R. Xu, W. Yang and M. Kraft, Extension of moment projection method to the fragmentation process. *J. Comput. Phys.* **335** (2017) 516–534.

[34] R.M. Ziff and E. McGrady, The kinetics of cluster fragmentation and depolymerisation. *J. Phys. A: Math. General* **18** (1985) 3027.